Journal of Translational Science

Research Article

ISSN: 2059-268X

Direct regional microvascular monitoring and assessment of blood brain barrier function following cerebral ischemia-reperfusion injury

Tavarekere N Nagaraja[1,2*], Kelly A Keenan[1,2], James R Ewing[3,4], Sukruth Shashikumar[2], Varun S Nadig[2], Raveena Munnangi[2] and Robert A Knight[3,4]

[1]Department of Neurosurgery, Henry Ford Hospital, Detroit, MI, USA

[2]Department of Anesthesiology, Henry Ford Hospital, Detroit, MI, USA

[3]Department of Neurology, Henry Ford Hospital, Detroit, MI, USA

[4]Department of Physics, Oakland University, Rochester, MI, USA

Abstract

Evans Blue (EB) is often used to evaluate Blood-Brain Barrier Damage (BBB) in cerebral ischemia, frequently by dye extraction. Herein we present a method that allows assessing regional brain microvasculature, distribution of EB and Fluorescent Isothiocyanate-Labeled Red Blood Cells (FITC-RBCs) in a rat model of acute cerebral Ischemia-Reperfusion (I-R). Wistar rats were subjected to 3 h of middle cerebral artery occlusion and then reperfused. At ~2.5 h of reperfusion, BBB opening was assessed by contrast enhanced magnetic resonance imaging. It was followed by injections of EB and FITC-RBCs that circulated for either 5 or 20 min. Regional microvasculature and tracer distributions were assessed by laser scanning confocal microscopy. Microvascular networks in stroke-affected regions networks were partially damaged with apparent EB extravasation. Brain regions were affected in the following order: preoptic area (PoA)>striatum (Str)>cortex (Ctx). EB leakage increased with circulation time in Str. Cells around the leakage sites sequestered EB. An inverse correlation was observed between low CBF rates recorded during MCA occlusion and post-reperfusion EB extravasation patterns. Accordingly, this approach provided data on brain regional microvascular status, extravascular tracer distribution and its cellular uptake. It may be useful to evaluate model-dependent variations in vascular injury and efficacy of putative vascular protective drugs in stroke.

Introduction

Ischemia-Reperfusion (I-R)-induced BBB opening is known to worsen neuronal injury in its vicinity and the degree and location of such opening is believed to portend the development of hemorrhagic transformation [1]. Therefore, evaluation of acute BBB damage is important in determining the course of thrombolytic therapy and for treatment of the neurovascular unit (NVU) to achieve a favorable outcome after cerebral ischemia. Thus, vascular protection as a means of augmenting neuroprotection is now considered a valid strategy in stroke treatment [2].

Both non-invasive and terminal techniques are available for the evaluation of BBB damage. Contrast enhanced magnetic resonance imaging (CE-MRI) is a frequently used technique for non-invasive evaluation of acute BBB opening after stroke in both experimental studies and humans [3-5]. Experimental stroke studies may also involve intravenous injection of a tracer dye such as Evans blue (EB) for evaluation of microvascular damage, often by extraction and spectrophotometric estimation of dye content of the tissue [6-14]. Increased tissue tracer concentration in comparison to controls would then indicate elevated vascular permeability to the tracer. However, dye extraction leads to loss of all data at the microcirculatory level about the relative status of the vasculature among the affected regions, regional variations in the magnitude of tracer distribution and on possible cellular uptake of the dye. EB binds to plasma albumin after injection and is presumed to represent plasma flow. Imaging-based quantification of EB distribution has been reported, but few studies have reported the effects of acute BBB permeability changes in stroke on parenchymal and cellular distribution of EB and of red blood cells (RBCs) among different brain regions [15].

This study employed a laser scanning confocal microscopy (LSCM)-based method for evaluating brain regional EB extravasation after increased cerebrovascular permeability following unilateral transient cerebral ischemia. The rats were injected with EB and fluorescent isothiocyanate (FITC) labeled RBCs after MRI and brain slices were examined for corresponding tracer distribution patterns. Increased BBB permeability in the hemisphere ipsilateral to stroke injury was confirmed by CE-MRI that preceded tracer injection and microscopy. It was hypothesized and tested that the extent of BBB opening will vary in its magnitude among different brain regions exhibiting stroke injury and that LSCM-imaging technique will underscore such variations.

Correspondence to: Dr. Tavarekere N. Nagaraja, Department of Neurosurgery, Henry Ford Hospital, 2799 West Grand Blvd., Detroit, MI 48202, Tel: (313) 916-3853; Fax: (313) 916-1324; **E-mail:** tnagara1@hfhs.org

Key words: *evans blue, FITC, laser scanning confocal microscopy, magnetic resonance imaging, rat, Stroke*

Received: August 23, 2015; **Accepted:** September 14, 2015; **Published:** September 17, 2015

Materials and methods

Animal preparation and surgery

All experimental protocols were approved by the Institutional Animal Care and Use Committee. Eight male Wistar rats weighing ~300 g were randomly assigned to one of two experimental groups. The rats were anesthetized with 3.0% halothane, and then maintained with 0.75-1% halothane in a 2:1 N_2O:O_2 mixture using a facemask. Body temperature was maintained at 37°C using a water-heated recirculating rubber mat and monitored via an intrarectal thermocouple (Kent Scientific, Torrington, CT, USA). The right femoral artery and vein were cannulated using polyethylene–50 tubing (Becton Dickinson & Co., Sparks, MD, USA) for measuring arterial blood gases and blood pressure during the occlusion and reperfusion periods and for intravenous injection of MRI contrast agent and fluorescent tracers, respectively.

The right middle cerebral artery (MCA) was occluded by an intraluminal filament for 3 h after which reperfusion was begun by suture withdrawal using methods described previously [16-18]. Prior to MCA occlusion, 1.0 ml of arterial blood was collected to isolate and prepare FITC-RBCs for injection later. The lost blood volume was immediately replaced with normal saline. During the period of MR imaging, RBCs were labeled with FITC using a kit (Molecular Probes, Eugene, OR, USA) following published procedures [19].

Magnetic resonance imaging

All studies were performed using a 7 Tesla, 20 cm bore superconducting Magnex magnet (Magnex Scientific Inc., Abingdon, UK) interfaced to a Bruker console (Bruker Biospin MRI, Inc. Billerica, MA, USA) and equipped with a 12 cm self-shielded gradient set capable of producing 25 gauss/cm gradients with 100 μs rise times. Estimates of cerebral blood flow (CBF), apparent diffusion coefficient of water (ADC, using data from diffusion-weighted imaging) and T_2 were acquired from 45 to 120 min after MCA occlusion as described previously [17,20-22].

After 3 hrs of occlusion, the animal was removed from the magnet, and the suture occluding the MCA was withdrawn to begin reperfusion. The rat was then quickly placed back in the magnet for post-reperfusion CBF and T_2-weighted imaging (T_2WI) that were acquired from 30-120 min thereafter. About 20 min later, CE-MRI, with an intravenous injection of gadolinium diethylene triaminepentaacetic acid (Gd-DTPA), was performed.

Gd-DTPA administration and T_1 Look-Locker (L-L) imaging

Gd-DTPA was prepared in-house following published methods at a stock solution concentration of 400 mmol [23]. Baseline T_1-weighted spin-echo (TR/TE = 1000 ms/20 ms) and L-L scans were collected prior to contrast administration. After obtaining one or two baseline estimates, Gd-DTPA was injected as a bolus through the femoral vein at a dose of 80 μmol/kg body weight. Estimates of T_1 were acquired using the L-L T_1 procedure to generate maps of the longitudinal relaxation rate R_1 ($R_1=1/T_1$) at approximately 3 minute intervals for the next 21 min. Temporal data was obtained for five interleaved 2 mm thick slices. At the conclusion of the L-L series, a final post-contrast T_1-weighted multislice spin-echo image set was obtained.

MR data analysis

The MR images were processed using a SUN workstation (Sun Microsystems, Santa Clara, CA) to generate pre and post contrast T_1-weighted images (T_1WI). The pre-contrast baseline images were subtracted from the post-contrast images to identify regions of Gd-DTPA enhancement (T_1-subtraction images). Quantitative maps of CBF, ADC and T_2 were also generated from the raw data using previously published methods and their values were expressed as ipsi/contralateral (I/C) ratios [22].

Tissue preparation for LSCM

After completion of the CE-MRI series, the rats were removed from the magnet and were injected with Evans blue (0.2 ml/100g body weight of a 2% solution in normal saline) and 1.0 ml of FITC-RBCs in normal saline. The two tracers were allowed to circulate for a period of either 5 (n = 4) or 20 min (n = 4), respectively, and the rats were then killed by decapitation under deep halothane anesthesia. A blood smear preparation was done to ensure the presence of FITC-RBCs.

Brains were removed immediately after sacrifice and immersed in 10% buffered formalin (VWR Intl., West Chester, PA, USA) for 48 hours and then block-cut into serially labeled, coronal, 2 mm thick slices using a rat brain matrix (ASI Instruments, Inc., Warren, MI, USA). The slices showing blue coloration indicating EB leakage were photographed for visual comparison with the central MR slice showing Gd-DTPA enhancement. The slices were then placed into separate tissue cassettes and fixed in 4% paraformaldehyde overnight. From these slices 100 μm thick coronal sections were cut using a vibratome (Technical Products Intl. Inc., St. Louis, MO, USA). The slices were mounted on individual slides and coverslipped with Glycergel (Dako, Carpenteria, CA, USA).

Image acquisition

The vibratome sections were analyzed using a Bio-Rad MRC 1024 (argon and krypton) laser-scanning confocal imaging system mounted onto a Zeiss microscope (Bio-Rad, Cambridge, MA, USA). Microscopic data were acquired using a 10x objective (numerical aperture = 0.3) and a 40X oil immersion objective lens (numerical aperture = 1.3). FITC-RBCs (green fluorochrome) and EB-labeled microvessels (red fluorochrome) were excited by a laser beam at 488 and 568 nm, respectively, and emissions were detected with a photomultiplier tube through 522 and 585 nm emission filters, respectively. Laser intensity was set at 10% of laser power and offset/black level at zero for all data acquisition. Electronic gain was set at 1000 for the two photomultiplier tubes and the iris/confocal aperture adjusted from 4.3-4.5 for FITC and from 2.5-3.0 for EB. Because the size of the fluorescent beam in a xy-dimensional image depends on laser power, iris, gain, and duration of sampling time, these parameters were kept constant during data acquisition.

Based on MR maps, three regions of interest (ROIs) including areas within i) the preoptic area (PoA), ii) the striatum (Str) and iii) cortex (Ctx; mainly parietal and/or insular cortices adjacent to Str) were selected and examined in both contralateral hemisphere and corresponding ischemic hemisphere of each animal. Images from the contralateral hemisphere were considered as the control in each experiment for comparison. For both hemispheres, high resolution images (using a 40x objective) from five areas in each of the ROI were obtained in 512 x 512 pixel format in the x-y direction using a 4x frame-scan average. 30 thin optical sections were acquired along the z-axis with a 1-um step size using a 40x objective lens.

Image analysis

An imaging system (Micro Computer Imaging Device; Imaging

Research, St. Catherines, ON, Canada) was used to process images from the laser scanning confocal microscope to measure FITC-labeled RBCs and Evans blue-albumin perfused vessels and leakage.

Linear distance was calibrated vertically and horizontally at the beginning of each session using a 300 mesh square electron microscopy grid. Each of the 30–40x magnification z-series images from an area was imported into the system on separate channels, and a fixed 256-gray-scale display cutoff was applied to ensure that an accurate rendering of the original vessel staining pattern was obtained. A threshold was set for each of the three contralateral ROIs to match published values for radiolabeled albumin distribution according Bereczki, *et al.* [24]. Following this convention, the contralateral EB space was set to 0.45% of the target area for preoptic area, 0.58% for lateral caudate-putamen, and 0.80% for the neocortex. Corresponding ROI images from the ipsilateral hemisphere areas were collected at identical settings so that their values represented variations from normal due to prevailing I-R conditions.

The images imported into the system allowed for a single projected composite image to be reconstructed from the single images of both EB and FITC-labeled RBCs obtained separately earlier. Since the z-step position was kept intact, the resulting reconstructions covered identical tissue volumes and could be overlaid to produce composite images. The ensuing data were expressed as ratios of contralateral values and are represented as the following parameters: i) Leakage, percentage of fields with disrupted vasculature and a hazy background; ii) Fields, percentage of fields with extravascular accumulation of EB with no evident cellular uptake; and iii) Uptake, percentage of fields with cellular uptake of EB. Each ROI was evaluated in 5 brain slices from each rat independently by three investigators for these three parameters, the values were averaged and the mean value was considered as representative of that ROI. All data are shown as mean ± standard error of mean. They were analyzed using t-tests and Pearson's correlation coefficients with significance inferred at $p<0.05$.

In separate experiments, timed arterial blood samples were collected after an intravenous bolus injection of EB. Plasma EB concentrations in these samples were measured using a curve of EB standards versus their optical density in a microplate reader (ELx800, Bio-Tek Instruments, Inc., Winooski, Vermont, USA) at 630 nm. An arterial time-concentration curve of EB was produced using these data.

Results

General observations

Apart from a slight hypercapnia after MRI, measured physiological parameters in all the animals were within the normal range (Table 1). Ischemia was confirmed by the reduction of CBF during MCA occlusion; magnitude of reperfusion was recorded by the extent of restitution of CBF in such regions after suture withdrawal (Figures 1A and 1B). Brain areas usually affected in this stroke model are PoA, Str and Ctx, and they constituted the three ROIs for further examinations. CBF reductions during MCA occlusion were about 75%, 70% and 40% in PoA, Str and Ctx, respectively, compared to the CBF values from their corresponding contralateral regions. CBF restitution after reperfusion varied among these regions, with estimated deficits after reperfusion being approximately 50%, 40% and 5% in PoA, Str and Ctx, respectively. Differences between CBF during occlusion and reperfusion were significant for all three ROIs (Table 2). I/C ratios of T_2 were elevated and those of ADC were decreased in accordance with the prevailing ischemic conditions in these ROIs, but of them only differences in ADC in PoA and Str were significant (Table 2). More rats showed damage in PoA than in Str and Ctx (Table 3).

Table 1. Physiological status of the rats (n=8) during and after magnetic resonance imaging.

	Time	
Parameter	During MRI	After MRI
pH	7.4 ± 0.03	7.3 ± 0.11
pCO_2[a]	30.3 ± 1.53	44.6 ± 1.50
pO_2[b]	116.1 ± 6.54	101.9 ± 8.18
Temp[c]	37.1 ± 0.07	37.0 ± 0.25
MAP[d]	94.7 ± 2.53	104.2 ± 4.18
Glucose[e]	-----	163.0 ± 6.00
Osmolality[f]	-----	304.1 ± 0.93
Hematocrit	-----	0.4 ± 0.10

Values are given as mean ± standard error of mean. [a, b]partial pressures in mm Hg; [c]rectal temperature in °C; [d]mean arterial pressure in mm Hg; [e]mg/100 ml plasma; [f]mOsm/kg H_2O; -----not measured.

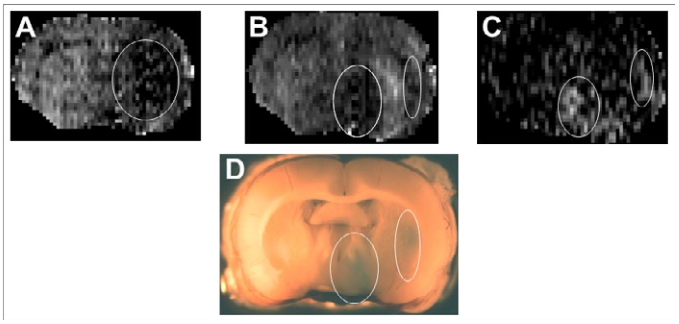

Figure 1. A typical set of MR images and the corresponding Evans blue stained brain section from an experiment. From left to right, the first two are the coronal CBF images of the brain during occlusion (A) and reperfusion (B) and the third is a T_1 subtraction image showing the region of contrast enhancement (C).The dark region outlined in the right hemisphere in A is ischemic. It is seen that following reperfusion cerebral blood flow is restored in the center of this lesion flanked by two separate regions with sustained low blood flow (bright pixels in the middle of the two ovals in B). In the T_1 subtraction image, two distinct regions of contrast enhancement (two ovals in C) indicating ischemia-induced acute blood-brain barrier opening are visible. These two ovals spatially correspond with the two regions with low blood flow shown in the reperfused brain in the middle panel. The 2 mm brain vibratome slice corresponding to the MR images is also shown (D) wherein blue regions of EBA leakage are visible on the ipsilateral side (oval outlines in D that spatially correspond to the 2 ovals in C).

Table 2. Summary of the measured magnetic resonance imaging parameters during ischemia and reperfusion (n=8).

Parameter	ROI[a]	Time	
		Occlusion	Reperfusion
CBF	PoA[b]	0.23 ± 0.06	0.48 ± 0.10[e]
	Str[c]	0.32 ± 0.07	0.63 ± 0.11[e]
	Ctx[d]	0.60 ± 0.10	0.95 ± 0.08[f]
T_2	PoA	1.31 ± 0.06	1.53 ± 0.11
	Str	1.19 ± 0.06	1.42 ± 0.09
	Ctx	1.21 ± 0.04	1.26 ± 0.05
ADC	PoA	0.71 ± 0.07	1.1 ± 0.08[g]
	Str	0.80 ± 0.11	1.02 ± 0.07[h]
	Ctx	1.05 ± 0.03	0.94 ± 0.04

All values are given as mean ± standard error of mean of ipsilateral-to-contralateral ratios. CBF, cerebral blood flow; T_2, transverse relaxation time; ADC, apparent diffusion coefficient of water; [a]region of interest; [b]preoptic area; [c]striatum; [d]cortex; [e]$p = 0.02$; [f]$p = 0.03$; [g]$p = 0.001$; [h]$p = 0.05$ (Paired t-tests)

Table 3. Fraction of rats showing vascular injury at the two tracer circulation time points for the three ROIs in terms of the three chosen parameters.

ROI	Time	Leakage*	Fields*	Uptake*
PoA	5 min	4/4	4/4	3/4
	20 min	4/4	4/4	4/4
Str	5 min	2/4	1/4	1/4
	20 min	3/4	2/4	3/4
Ctx	5 min	2/4	1/4	0/4
	20 min	1/4	1/4	1/4

*Leakage indicates extravasation of EB including a hazy background; *Fields indicates visible extracellular presence of EB; *Uptake indicates cellular uptake of EB.

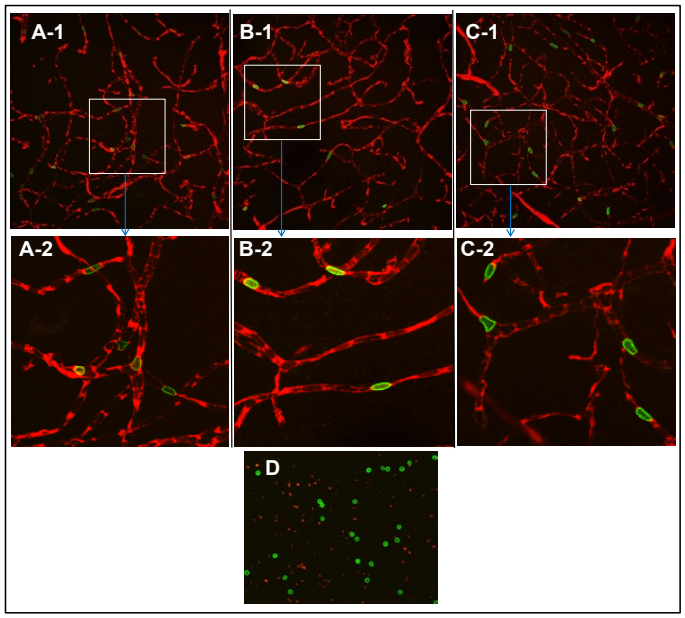

Figure 2. Contralateral microvasculature from the three ROIs examined using a 40X objective: PoA (A-1), Str(B-1), Ctx (C-1); an example of a blood smear preparation examined with a 10X objective (D); and enlarged images of boxes in A-1, B-1 and C-1 (A-2, B-2 and C-2,respectively). Intact, interconnected vascular networks are visible in A-1, B-1 and C-1 with a dark background suggesting the absence of any tracer extravasation. The vessels are filled with plasma labeled red by EB with FITC-RBCs traversing it and seen as distinct, intravascular green spots in all three ROIs. Abrupt endings of vascular segments indicate their extension perpendicularly beyond the foci of imaging plane. The smear preparation in D shows bright green, intact, circular RBCs. Their low density reflects the partial population of RBCs labeled with FITC; the red speckles are EB-stained plasma components in blood. The enlarged images in A-2, B-2 and C-2 show some examples of the adaptive deformations of RBCs (58) to facilitate their flow within the microvasculature.

Microvascular status

Extravascular enhancement of Gd-DTPA was observed in at least one ROI in all experiments, confirming localized BBB opening after reperfusion (Figure 1C). Macroscopic examination of the corresponding 2 mm thick brain slices showed blue coloration indicating subsequent EB leakage as well in these regions (Figure 1D). An examination of images from contralateral hemisphere showed intricately interconnected vascular networks (Figures 2A1-C1). Microvessels were filled with plasma labeled by EB that fluoresced red and FITC-RBCs were seen as green circles or ovals within the plasma (Figures 2A1-2C1). The cortex seemed to display relatively denser and more complex vascular organization per visual evaluation, but this needs to be confirmed by future quantitation. The blood smear preparation showed a population of intact, FITC-labeled RBCs (Figure 2D). The adaptive deforming capacity of RBCs during their transit could be discerned by a comparison of the circular cells seen in 2D with the intravascular FITC-RBCs shown magnified in Figures 2A-2, 2B-2 and 2C-2 that appear either oval, oblong or otherwise squeezed, very likely to conform to the microvascular lumen. Unlabeled RBCs were perceived as dark gaps in the red EB fluorescence.

In comparison to their corresponding contralateral vasculature (Figure 3: A-1, B-1, C-1), ipsilateral vasculature displayed damaged microvessels with EB leakage (Figure 3: A-2, B-2, C-2 and A-3, B-3, C-3). The extravascular EB was visible as a hazy background and/or dispersed red patches among the capillary network. These patches varied in size and shape among the ROIs, with no given ROI showing any particular pattern of distribution. A notable feature in several leakage regions was the cellular uptake of EB. Such cells were discernible amongst the

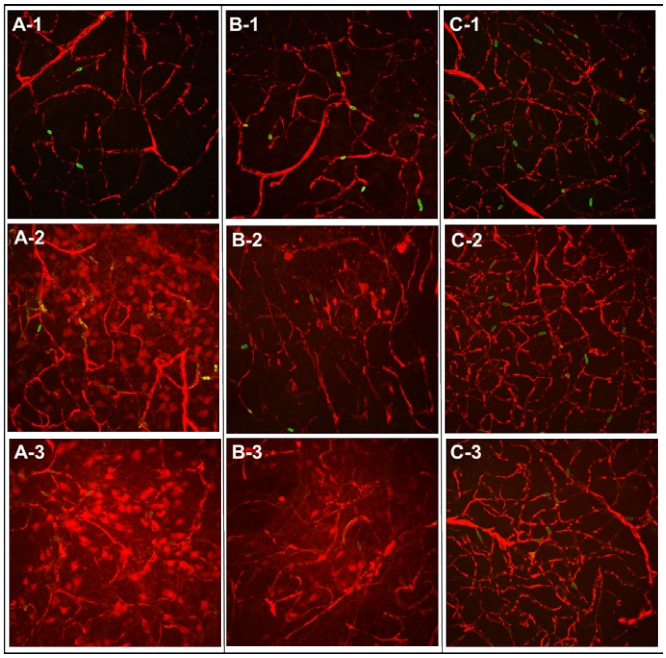

Figure 3. Laser scanning confocal microscopic images of microvascular structures after 5 or 20 min of EB and FITC-RBCs circulation examined using a 40X objective. Images in the top row (A-1, B-1, C-1) are from the contralateral hemisphere after 20 min circulation and serve as references for the two sets of panels below, that are from the ischemic hemisphere after 5 (A-2, B-2, C-2; middle row) or 20 min (A-3, B-3, C-3; bottom row) of tracer circulation. From left to right, the three columns of images are from PoA (A-1, A-2, A-3), Str (B-1, B-2, B-3) and Ctx (C-1, C-2, C-3). Vasculature is labeled by red Evans blue fluorescence within which circular or oval green spots of FITC-labeled RBCs are visible. Intricate and intact vascular networks with a dark background indicating no vascular leakage can be seen in the top panel images from the contralateral hemisphere. In the 5 min circulation image from PoA in the middle panel (A-2), the network is damaged and a large number of cells have taken up EB. Fewer such cells are visible in Str at this time along with a red haze suggesting sizeable interstitial EB distribution (B-2). The cortical network, however, seems to be the least damaged with no apparent extravascular presence of EB (C-2). Note the FITC-RBCs in all images are intravascular.In the image after 20 min of tracer circulation from PoA (A-3) shown in the bottom panel, the network is damaged further and a larger number of cells are labeled by leaked EBA along with the interstitium also appearing hazy with a reddish tint, presumably due to the longer period of EB extravasation. The red haze in Str (B-3) is also stronger compared to that in B-2, probably due to the same reason.The cortical network, however, seems still intact albeit with a relatively hazier background (C-3; please note that although one rat showed cortical vascular damage, a more representative example of less extensive cortical injury was chosen for illustration). Note the FITC-RBCs in all images from the bottom panel are also still intravascular.

extravascular EB patches as brighter, localized spots of fluorescence either widely distributed or in small clusters (Figure 3: A-2, A-3, B-2, B-3). Neither EB leakage nor cellular uptake was observed in the contralateral regions. Further examination of EB distribution showed several unique features in its distribution depending on the ROI and the circulations times. Figure 4 depicts them for each of the three ROIs. Briefly, PoA was more susceptible to microvascular damage than Str, Ctx being the least damaged. Leakage and Fields expanded in Str and Ctx during the increase in tracer circulation duration from 5-20 min.

Using Pearson correlation coefficients, relationships between MRI signatures of stroke damage and fluorescence microscopic parameters were examined to test whether any imaging biomarker could be predictive of impending tissue injury (Figure 5: A-1, A-2, B-1, B-2). From the combinations tested, an inverse correlation was found between CBF during occlusion and the magnitude of EB leakage in PoA (Figure 5: A-1) and Str (Figure 5: B-1); this relationship persisted post-reperfusion in the PoA (Figure 5: A-2), but was not observed in Str (Figure 5: B-2).

In the EB time-concentrations curves, blood levels of EB held relatively steady for the duration of observation. After an initial peak and exponential decline to about 70% of peak value in the first few minutes, they declined very slowly toward 50% peak value over a period of 3 hrs (Figure 6).

Discussion

These data present the varied microvascular patterns that characterize cortical and subcortical brain regions and the effects of transient, 3 h MCA occlusion on their gross morphology in normal

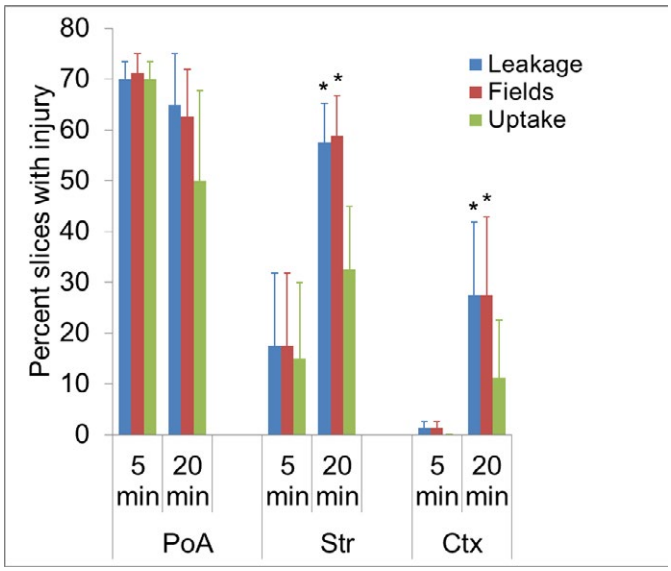

Figure 4. A bar graph depicting the percent values of leakage, fields with EB accumulation and EB cellular uptake. The different experimental cohorts are shown along the abscissa and the magnitude of measured index of injury along the ordinate. Five slices were evaluated in each rat giving a total sample of 20 per time group.A majority of such brain slices were damaged in PoA and parameter value numbers did not significantly change between the two circulation durations. However, in Str, although all three parameters showed increases, only changes in leakage and fields were statistically significant for the 20 min group compared to its 5 min cohort.No evidence of vascular damage was seen in Ctx in the 5 min cohort and just one rat showed cortical vascular disruption in the 20 min circulation group. All 5 slices (25% of the total) examined in it demonstrated EB extravasation and the increases between 5 min and 20 min groups were statistically significant for two of the three parameters evaluated. *p<0.05 (Student's t-test).

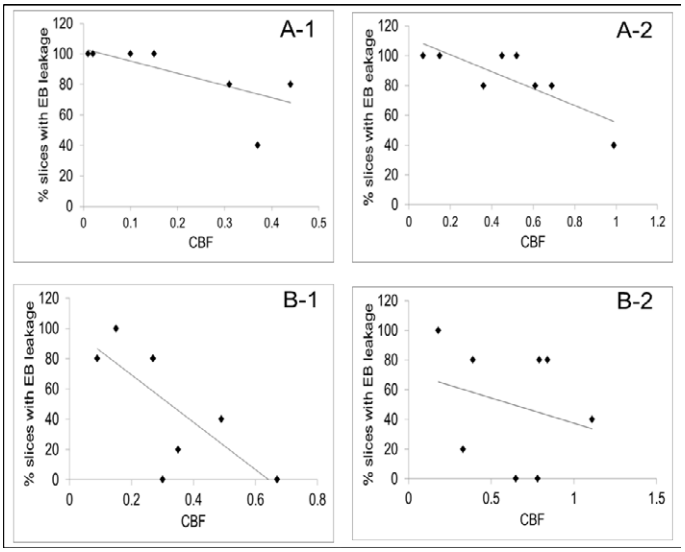

Figure 5. Scatter plots showing the correlations between CBF and EB leakage in PoA (A-1, A-2) and Str (B-1, B-2). Ipsi-to-contralateral CBF ratios are shown along the abscissa and the percent slices with EB extravasation along the ordinate.An inverse relationship was observed between CBF and injury during occlusion in PoA (A-1; R^2=0.5; Pearson coefficient = -0.7; p<0.05) and Str (B-1; R^2=0.5; Pearson coefficient = -0.7; p<0.05). A similar relationship was observed in PoA after reperfusion (A-2; R^2=0.7; Pearson coefficient = -0.8; p<0.05), but not in Str (B-2; R^2=0.07; Pearson coefficient -0.2; p<0.50).

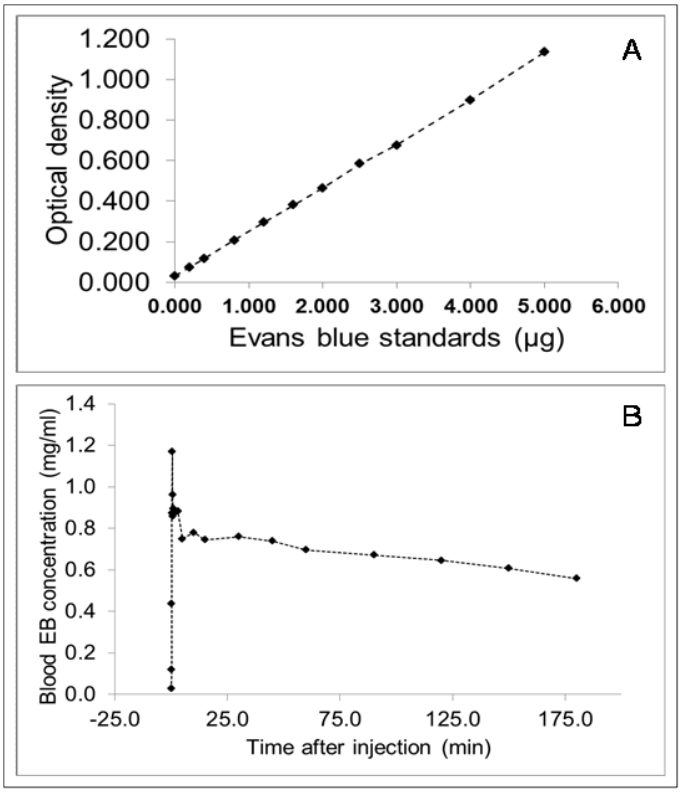

Figure 6. Plots showing Evans blue measurements. A typical standard curve obtained with known EB concentrations plotted against their optical density is shown in A. A plot of blood levels of EB for 3 h after an intravenous injection is shown in B. It can be seen that EB, owing to its binding to plasma albumin, maintains a steady level for an extended duration after the initial peak immediately following injection.

rats. Evans blue, a dye frequently used in BBB investigations was employed as the tracer of choice to illustrate the patterns. Autologous, FITC-labeled RBCs were concurrently injected to demonstrate the relative tightness of the breached barrier to blood-borne cellular elements at this time of acute reperfusion. The resultant data suggest that a quantitative analysis of EB leakage that preserves microvascular status can be performed in experimental stroke studies. Fluorescent tracers such as EB are frequently employed to evaluate BBB damage in cerebral ischemia, most often by dye extraction and its colorimetric quantification. This approach gives accurate dye content of tissue, but leads to the loss of very important data on brain regional microvascular status and, in addition, any differences in dye distribution among stroke-affected brain regions and possible cellular uptake of the dye therein are also lost. Therefore, an imaging-based technique that generates several parameters of interest such as its region-specificity, microvascular status, tracer extravasation patterns and cellular uptake can be more advantageous in evaluating stroke injury. Uptake of extravasated EB has been previously reported following cold injury and transient ischemia [25-27]. Although the subtypes of such cells were not further explored in our study, EB uptake by both neuronal and non-neuronal cells is known [25-27]. The FITC-RBCs seemed to be confined to intravascular space in all regions, supporting previous observations that hemorrhagic transformation was not part of the pathology at this time [1].

Some studies have employed a somewhat similar approach to estimate EB extravasation to measure vascular dysfunction. After an intravenous injection of EB, its extravasation from dural vessels due to unilateral trigeminal ganglion stimulation was measured by confocal laser scanning microscopy of the fixed dura mater [28]. EB intensity from several ROIs on the ipsilateral side was compared to that from the contralateral side to generate a ratio of fluorescence increase that reflected plasma protein extravasation. The values obtained were comparable to previously reported values from experiments that used radioactive albumin as the tracer [28]. Klohs and co-workers used near-infrared fluorescence (NIRF) imaging of bovine serum albumin to visualize BBB opening in a mouse model of MCA occlusion. The NIRF imaging strongly correlated with the amount and temporal patterns of extravasated EB. However, evaluation of microvasculature was not possible with this method and the detection capability may also be limited to thinner skulls in mouse models. An optical imaging method to measure EB leakage in a rat thromboembolic stroke model has also been reported [15]. This method seems to provide information on regional variations in leakage, but without microvascular status and interstitial tracer distribution directionality. Intravital imaging with LSCM has been used by some authors to measure flow changes in the cortex using a cranial window technique or skin preparations [29]. Several fluorescent dyes, including EB, have been used to measure flow variations as a result of an injury or drug treatment in live, anesthetized animals. While very informative, such techniques may be limited to about 200 μM of tissue depth that the laser beam can access. It is also known that increments in laser intensity can themselves cause endothelial damage [30]. In contrast, although terminal, the present techniques provided relevant data on microvascular network patterns, plasma and RBC regional distributions and extravascular cellular uptake of plasma-borne tracers. A somewhat similar approach was employed by Morris et al. who used fluorescent dextran in sequence with EB to differentiate between reperfused and unreperfused vasculature in cerebral ischemia [31].

One of the observations in this study was the gradation in susceptibility among cortical and subcortical regions in this model that support our and others' previous observations [27,32,33]. Unlike in Str and Ctx, leakage patterns did not increase in PoA from 5 to 20 min circulation suggesting it is affected very early in the disease cascade. The absence of further increase in damage may be due to the maximum extent of effects already happening in this region. Moreover, unlike many other intravenous tracers, due to its albumin binding, EB maintains a relatively steady blood level for a significant duration after a single bolus injection (Figure 6); therefore, the continued reduction in CBF could have limited the delivery of the tracer and led to lesser extravasation despite an open BBB and tracer availability. The decrease in the number of cells labeled by EB in PoA from 5 to 20 min was probably due to ongoing cell death and lysis. All three parameters showed increases from 5 to 20 min in Str, due to the relative tightness of the BBB that required longer circulation duration to manifest its breach. Also note that post-reperfusion CBF restitution in Str was higher than in PoA (Table 2) and fewer animals showed Str abnormalities (Table 3). In contrast, Ctx demonstrated relative resilience to damage. Not only the measured MR indices were the least affected in it (Table 2), just two rats showed cortical vascular injury (Table 3). Due to the negligible amount of injury seen in the 5 min group, even though just one animal showed BBB damage, the increases at 20 min circulation turned out to be statistically significant (Figure 4). Another factor for the increase in the number of slices showing EB leakage may be tracer diffusion over the circulation period from the source of leakage.

Vascular pathophysiology in stroke has been the subject of some studies [33-35]. They have shown that neocortical structures possess more collateral that can compensate for localized flow reductions. Moreover, flow can also be 'plasmatic' in some loci with about 4% of capillaries showing no RBC flow [36]. Our data support these notions to some extent. Cortical vascular networks seemed denser and more complex than subcortical regions and there were several vascular segments in all three ROIs that seemed to show no FITC-RBCs (Figure 2). These observations, however, need to be confirmed in future studies by quantification. It may be premature to conclude that all segments that did not show the presence of FITC-RBCs were plasmatic since only a fraction of RBCs were FITC-labeled (about 2.0%, assuming a total blood volume of 20 ml and the measured hematocrit value of 40% (Table 1)). Nonetheless, such characterizations of cerebral vasculature in stroke, especially in the context of co-morbidities such as hypertension and diabetes that are known to affect cerebrovascular integrity in a region specific manner, are warranted if we are to develop therapies that address the complete NVU as the treatment target [37-40].

The correlation between decreased CBF and increased extravascular EB (Figure 5) confirms our previous observation that reduction in CBF during stroke seemed to determine impending BBB damage and the concept that 'time is brain' [41,42]. The present data indicate that in embolic stroke, restitution of CBF as quickly as possible is crucial in limiting ensuing brain damage. They also indicate that the extent of reduction in CBF may be a predictive biomarker for I-R-induced BBB damage in acute stroke along with permeability changes suggested to portend hemorrhage by other investigators [43]. However, our data suggest the extent of CBF reduction during occlusion could be the more robust and less region-specific predictor than after reperfusion. Acute CBF measurements may also provide an independent parameter for secondary confirmation of vascular injury when permeability measurements vary across different imaging modalities such as MRI and computed tomography [44].

The cellular uptake of extravascular EB raises some interesting questions. Can therapeutic molecules follow suit and, if so, is it possible to use such BBB openings as conduits for brain drug delivery in stroke [45]? Supporting such an assumption are reports of biphasic BBB opening in stroke [9,46-48]. It needs to be tested whether a transient breach in the barrier will allow the passage of small drug molecules. This approach may also have the additional advantages that the normal brain tissue with an intact BBB will not be exposed to the drug and that the known edema fluid flow across the stroke lesion may provide additional diffusion and bulk flow carriers for the drug [49,50]. It may be pertinent to note here that techniques to temporarily open the BBB for delivering drugs are being actively investigated [51-53].

MCA occlusion is a widely prevalent method for stroke studies and is being used to test several putative therapies [54]. The overall effects of such therapies have been usually measured in decreases in lesion size, neuronal morphology and motor functions, and a small number have focused on brain regional differences in such evaluations. Such differences, however, may be crucial in determining therapy efficacy. For instance, caffeinol therapy was reported to be protective in cortical regions with little effect on subcortical regions or on brain edema [32,55]. It is conceivable that the highly complex vascular architecture of the cortex with abundant collateral flow may have rendered it less susceptible to stroke injury, thus augmenting caffeinol's protective effects. Also important in this scenario is the observation that edema is likely to be more pronounced in subcortical than cortical regions in this stroke model. Presently, rather than the previously prevailing 'neurocentric' approach, inclusion of vascular protection as an essential component of stroke treatment is being recommended [56]. Implementing such recommendations will require inclusion of techniques for detailed analyses of cerebral microvasculature.

In summary, regional differences in stroke susceptibility and region-specific protective effects of some putative stroke treatments are known. Varying vascular dispositions in different parts of the brain are likely to contribute significantly to such differences. Thus, elucidation of ischemia-induced changes in microvascular status is vital for evaluating experimental therapies that aim to achieve cerebroprotection in stroke [57].

Acknowledgement

American Heart Association: Bugher Foundation Award 0270176N (RAK) & Scientist Development Grant 0635403N (TNN). The contents are solely the authors' and do not represent the official views of the American Heart Association. We are grateful to Dr. Joseph D. Fenstermacher for invaluable discussions on data analysis. We also thank: Dr. Stephen L. Brown and Andy Kolozsvary Jr. for FITC-RBC labeling; Jun Xu, Kevin Nelson and Richard L. Croxen for expert technical assistance; Nidhi N. Nadig and Neha Ray for help with graphs.

References

1. Knight RA, Barker PB, Fagan SC, Li Y, Jacobs MA, et al. (1998) Prediction of impending hemorrhagic transformation in ischemic stroke using magnetic resonance imaging in rats. *Stroke* 29: 144-151. [Crossref]

2. Ishrat T, Soliman S, Guan W, Saler M, Fagan SC (2012) Vascular protection to increase the safety of tissue plasminogen activator for stroke. *Curr Pharm Des* 18: 3677-3684. [Crossref]

3. Caplan LR, Arenillas J, Cramer SC, Joutel A, Lo EH, et al. (2011) Stroke-related translational research. *Arch Neurol* 68: 1110-1123. [Crossref]

4. Köhrmann M, Jüttler E, Huttner HB, Nowe T, Schellinger PD (2007) Acute stroke imaging for thrombolytic therapy--an update. *Cerebrovasc Dis* 24: 161-169. [Crossref]

5. Warach S, Latour LL (2004) Evidence of reperfusion injury, exacerbated by thrombolytic therapy, in human focal brain ischemia using a novel imaging marker of early blood-brain barrier disruption. *Stroke* 35: 2659-2661. [Crossref]

6. Bahcekapili N, Uzum G, Gokkusu C, Kuru A, Ziylan YZ (2007) The relationship between erythropoietin pretreatment with blood-brain barrier and lipid peroxidation after ischemia/reperfusion in rats. *Life Sci* 80: 1245-1251. [Crossref]

7. Candelario-Jalil E, Gonzalez-Falcon A, Garcia-Cabrera M, Leon OS, Fiebich BL (2007) Post-ischaemic treatment with the cyclooxygenase-2 inhibitor nimesulide reduces blood-brain barrier disruption and leukocyte infiltration following transient focal cerebral ischaemia in rats. *J Neurochem* 100: 1108-1120. [Crossref]

8. Kamada H, Yu F, Nito C, Chan PH (2007) Influence of hyperglycemia on oxidative stress and matrix metalloproteinase-9 activation after focal cerebral ischemia/reperfusion in rats: relation to blood-brain barrier dysfunction. *Stroke* 38: 1044-1049. [Crossref]

9. Klohs J, Steinbrink J, Bourayou R, Mueller S, Cordell R, et al. (2009) Near-infrared fluorescence imaging with fluorescently labeled albumin: a novel method for non-invasive optical imaging of blood-brain barrier impairment after focal cerebral ischemia in mice. *J Neurosci Methods* 180: 126-132. [Crossref]

10. Strbian D, Karjalainen-Lindsberg ML, Tatlisumak T, Lindsberg PJ (2006) Cerebral mast cells regulate early ischemic brain swelling and neutrophil accumulation. *J Cereb Blood Flow Metab* 26: 605-612. [Crossref]

11. Kahles T, Foerch C, Sitzer M, Schroeter M, Steinmetz H, et al. (2005) Tissue plasminogen activator mediated blood-brain barrier damage in transient focal cerebral ischemia in rats: relevance of interactions between thrombotic material and thrombolytic agent. *Vasc Pharmacol* 43: 254-259. [Crossref]

12. Hong SH, Khoutorova L, Bazan NG, Belayev L (2015) Docosahexaenoic acid improves behavior and attenuates blood-brain barrier injury induced by focal cerebral ischemia in rats. *Exp Transl Stroke Med* 7: 3. [Crossref]

13. Lok J, Zhao S, Leung W, Seo JH, Navaratna D, et al. (2012) Neuregulin-1 effects on endothelial and blood-brain-barrier permeability after experimental injury. *Transl Stroke Res* 3 Suppl 1: S119-124. [Crossref]

14. Van Winkle JA, Chen B, Lei IF, Pereira B, Rajput PS, et al. (2013) Concurrent middle cerebral artery occlusion and intra-arterial drug infusion via ipsilateral common carotid artery catheter in the rat. *J Neurosci Methods* 213: 63-69. [Crossref]

15. Jaffer H, Adjei IM, Labhasetwar V (2013) Optical imaging to map blood-brain barrier leakage. *Sci Rep* 3: 3117. [Crossref]

16. Longa EZ, Weinstein PR, Carlson S, Cummins R (1989) Reversible middle cerebral artery occlusion without craniectomy in rats. *Stroke* 20: 84-91. [Crossref]

17. Knight RA, Nagaraja TN, Ewing JR, Nagesh V, Whitton PA, et al. (2005) Quantitation and localization of blood-to-brain influx by MRI and quantitative autoradiography in a model of transient focal ischemia. *Magn Reson Med* 54: 813-821. [Crossref]

18. Nagaraja TN, Karki K, Ewing JR, Croxen RL, Knight RA (2008) Identification of variations in blood-brain barrier opening after cerebral ischemia by dual contrast-enhanced magnetic resonance imaging and T 1sat measurements. *Stroke* 39: 427-432. [Crossref]

19. Brown SL, Ewing JR, Nagaraja TN, Swerdlow PS, Cao Y, et al. (2003) Sickle red blood cells accumulate in tumor. *Magn Reson Med* 50: 1209-1214. [Crossref]

20. Ewing JR, Wei L, Knight RA, Pawa S, Nagaraja TN, et al. (2003) Direct comparison of local cerebral blood flow rates measured by MRI arterial spin-tagging and quantitative autoradiography in a rat model of experimental cerebral ischemia. *J Cereb Blood Flow Metab* 23: 198-209. [Crossref]

21. Knight RA, Karki K, Ewing JR, Divine GW, Fenstermacher JD, et al. (2009) Estimating blood and brain concentrations and blood-to-brain influx by magnetic resonance imaging with step-down infusion of Gd-DTPA in focal transient cerebral ischemia and confirmation by quantitative autoradiography with Gd-[14C]DTPA. *J Cereb Blood Flow Metab* 29: 1048-1058. [Crossref]

22. Nagaraja TN, Knight RA, Ewing JR, Karki K, Nagesh V, et al. (2011) Multiparametric magnetic resonance imaging and repeated measurements of blood-brain barrier permeability to contrast agents. *Methods Mol Biol* 686: 193-212. [Crossref]

23. Nagaraja TN, Karki K, Ewing JR, Divine GW, Fenstermacher JD, et al. (2010) The MRI-measured arterial input function resulting from a bolus injection of Gd-DTPA in a rat model of stroke slightly underestimates that of Gd-[14C]DTPA and marginally overestimates the blood-to-brain influx rate constant determined by Patlak plots. *Magn Reson Med* 63: 1502-1509. [Crossref]

24. Bereczki D, Wei L, Acuff V, Gruber K, Tajima A, et al. (1992) Technique-dependent variations in cerebral microvessel blood volumes and hematocrits in the rat. *J Appl Physiol* (1985) 73: 918-924. [Crossref]

25. Murakami K, Kawase M, Kondo T, Chan PH (1998) Cellular accumulation of extravasated serum protein and DNA fragmentation following vasogenic edema. *J Neurotrauma* 15: 825-835. [Crossref]

26. Remmers M, Schmidt-Kastner R, Belayev L, Lin B, Busto R, et al. (1999) Protein extravasation and cellular uptake after high-dose human-albumin treatment of transient focal cerebral ischemia in rats. *Brain Res* 827: 237-242. [Crossref]

27. Nagaraja TN, Keenan KA, Fenstermacher JD, Knight RA (2008) Acute leakage patterns of fluorescent plasma flow markers after transient focal cerebral ischemia suggest large openings in blood-brain barrier. *Microcirculation* 15: 1-14. [Crossref]

28. Schuh-Hofer S, Boehnke C, Reuter U, Siekmann W, Lindauer U, et al. (2003) A fluorescence-based method to assess plasma protein extravasation in rat dura mater using confocal laser scanning microscopy. *Brain Res Protocols* 12: 77-82. [Crossref]

29. Kenne E, Lindbom L (2011) Imaging inflammatory plasma leakage in vivo. *Thromb Haemost* 105: 783-789. [Crossref]

30. Dirnagl U, Villringer A, Einhäupl KM (1992) In-vivo confocal scanning laser microscopy of the cerebral microcirculation. *J Microsc* 165: 147-157. [Crossref]

31. Morris DC, Zhang Z, Davies K, Fenstermacher J, Chopp M (1999) High resolution quantitation of microvascular plasma perfusion in non-ischemic and ischemic rat brain by laser-scanning confocal microscopy. *Brain Res Brain Res Protoc* 4: 185-191. [Crossref]

32. Belayev L, Khoutorova L, Zhang Y, Belayev A, Zhao W, et al. (2004) Caffeinol confers cortical but not subcortical neuroprotection after transient focal cerebral ischemia in rats. *Brain Res* 1008: 278-283. [Crossref]

33. Del Zoppo GJ, Hallenbeck JM (2000) Advances in the vascular pathophysiology of ischemic stroke. *Thromb Res* 98: 73-81. [Crossref]

34. Del Zoppo GJ (1994) Microvascular changes during cerebral ischemia and reperfusion. *Cerebrovasc Brain Metab Rev* 6: 47-96. [Crossref]

35. Cavaglia M, Dombrowski SM, Drazba J, Vasanji A, Bokesch PM, et al. (2001) Regional variation in brain capillary density and vascular response to ischemia. *Brain Res* 910: 81-93. [Crossref]

36. Villringer A, Them A, Lindauer U, Einhäupl K, Dirnagl U (1994) Capillary perfusion of the rat brain cortex. An in vivo confocal microscopy study. *Circ Res* 75: 55-62. [Crossref]

37. Huber JD, VanGilder RL, Houser KA (2006) Streptozotocin-induced diabetes progressively increases blood-brain barrier permeability in specific brain regions in rats. *Am J Physiol - Heart & Circ Physiol* 291: H2660-H2668. [Crossref]

38. Hossmann KA (2006) Pathophysiology and therapy of experimental stroke. *Cell Mol Neurobiol* 26: 1057-1083. [Crossref]

39. Ginsberg MD (2009) Current status of neuroprotection for cerebral ischemia: synoptic overview. *Stroke* 40: S111-114. [Crossref]

40. Moskowitz MA, Lo EH, Iadecola C (2010) The science of stroke: mechanisms in search of treatments. *Neuron* 67: 181-198. [Crossref]

41. Nagaraja TN, Ewing JR, Karki K, Jacobs PE, Divine GW, et al. (2011) MRI and quantitative autoradiographic studies following bolus injections of unlabeled and [14] C-labeled gadolinium-diethylenetriaminepentaacetic acid in a rat model of stroke yield similar distribution volumes and blood-to-brain influx rate constants. *NMR Biomed* 24: 547-558. [Crossref]

42. Saver JL (2006) Time is brain--quantified. Stroke 37: 263-266. [Crossref]

43. Huang WY, Wu G, Li JJ, Geng DY, Tan WL, et al. (2015) Prediction of reperfusion-associated hemorrhagic transformation using dynamic contrast-enhanced imaging in a rat stroke model. *J Comput Assist Tomogr* 39: 787-793. [Crossref]

44. Merali Z, Wong T, Leung J, Gao MM, Mikulis D, et al. (2015) Dynamic contrast-enhanced MRI and CT provide comparable measurement of blood-brain barrier permeability in a rodent stroke model. *Magn Reson Imaging* 33: 1007-1012. [Crossref]

45. Lo EH, Singhal AB, Torchilin VP, Abbott NJ (2001) Drug delivery to damaged brain. *Brain Res Brain Res Rev* 38: 140-148. [Crossref]

46. Huang ZG, Xue D, Preston E, Karbalai H, Buchan AM (1999) Biphasic opening of the blood-brain barrier following transient focal ischemia: effects of hypothermia. *Can J Neurol Sci* 26: 298-304. [Crossref]

47. Kuroiwa T, Ting P, Martinez H, Klatzo I (1985) The biphasic opening of the blood-brain barrier to proteins following temporary middle cerebral artery occlusion. *Acta Neuropathol* 68: 122-129. [Crossref]

48. Rosenberg GA, Estrada EY, Dencoff JE (1998) Matrix metalloproteinases and TIMPs are associated with blood-brain barrier opening after reperfusion in rat brain. *Stroke* 29: 2189-2195. [Crossref]

49. Nagaraja TN, Keenan KA, Aryal MP, Ewing JR, Gopinath S, et al. (2014) Extravasation into brain and subsequent spread beyond the ischemic core of a magnetic resonance contrast agent following a step-down infusion protocol in acute cerebral ischemia. *Fluids Barriers CNS* 11: 21. [Crossref]

50. Reulen HJ (2010) Bulk flow and diffusion revisited, and clinical applications. *Acta Neurochir Suppl* 106: 3-13. [Crossref]

51. Zheng S, Bai YY, Liu Y, Gao X, Li Y, et al. (2015) Salvaging brain ischemia by increasing neuroprotectant uptake via nanoagonist mediated blood brain barrier permeability enhancement. *Biomaterials* 66: 9-20. [Crossref]

52. Neuwelt E, Abbott NJ, Abrey L, Banks WA, Blakley B, et al. (2008) Strategies to advance translational research into brain barriers. *Lancet Neurol* 7: 84-96. [Crossref]

53. Patel MM, Goyal BR, Bhadada SV, Bhatt JS, Amin AF (2009) Getting into the brain: approaches to enhance brain drug delivery. *CNS Drugs* 23: 35-58. [Crossref]

54. Lo EH (2008) Experimental models, neurovascular mechanisms and translational issues in stroke research. *Br J Pharmacol* 153 Suppl 1: S396-405. [Crossref]

55. Aronowski J, Strong R, Shirzadi A, Grotta JC (2003) Ethanol plus caffeine (caffeinol) for treatment of ischemic stroke: preclinical experience. *Stroke* 34: 1246-1251. [Crossref]

56. Fagan SC, Hess DC, Machado LS, Hohnadel EJ, Pollock DM, et al. (2005) Tactics for vascular protection after acute ischemic stroke. *Pharmacotherapy* 25: 387-395. [Crossref]

57. Maiese K (2001) The dynamics of cellular injury: transformation into neuronal and vascular protection. *Histol Histopathol* 16: 633-644. [Crossref]

58. Smith JE, Mohandas N, Shohet SB (1979) Variability in erythrocyte deformability among various mammals. *Am J Physiol* 236: 725-730. [Crossref]